CO_2 Capture Partner Molecules in Highly Loaded PEI Sorbents

Journal:	*The Journal of Physical Chemistry*
Manuscript ID	jp-2017-075416.R1
Manuscript Type:	Article
Date Submitted by the Author:	01-Sep-2017
Complete List of Authors:	Koutsianos, A; Swansea university, Energy Safety Research Institute Barron, Andrew; Rice University, Chemistry Andreoli, Enrico; Swansea University,

CO_2 Capture Partner Molecules in Highly Loaded PEI Sorbents

Athanasios Koutsianos[a], Andrew R. Barron[a,b,c], Enrico Andreoli[a,*]

[a] Energy Safety Research Institute, Swansea University, Bay Campus, Swansea, SA1 8EN,

[b] Department of Chemistry, Rice University, Houston, TX 77005, USA

[c] Department of Materials Science and Nanoengineering, Rice University, Houston, TX 77005, USA

* e.andreoli@swansea.ac.uk; +44(0)1792602524

Abstract

Decoupling amine loading from diffusion resistance is one of the main challenges in the development of immobilised amines CO_2 sorbents. Water has been reported to serve this goal alleviating CO_2 diffusional hindrance in highly loaded amine sorbents. Acting as a mass transport facilitator, water is not the only partner molecule able to enhance bulk CO_2 diffusion. Herein, we show that the enhancing effect of methanol is comparable to that of water in polyethyleneimine-based sorbents. Other molecules, such as ethanol, isopropanol, and chloroform, were also examined but did not appear to facilitate CO_2 transport and uptake. Based on a comparison of the Hansen solubility parameters of these molecules, it appears that polarity plays a crucial role in enhancing CO_2 diffusion together with molecular hindrance, and hydrogen bonding to a lesser extent.

Introduction

With the Paris agreement, a major step forward has been taken towards tackling climate change. Governments from all over the world agreed on a joint pledge to reduce annual greenhouse gas emissions to 40 billion tonnes of CO_2 equivalent ($GtCO_2eq$) by 2030, to be on a path of preventing global average temperature to exceed 2 °C above pre-industrial levels.[1] Green technologies are thus consistently gaining momentum. However, recent studies suggest that we/globally are unlikely to stop relying on fossil fuels as a primary energy source in the short or mid-term.[2] For this reason, CO_2 removal from power plants flue gases and stationary sources remains imperative.

To this end, we developed a solid sorbent material based on the cross-linking of polyethyleneimine (PEI) following an alternative approach where amino polymers are cross-linked instead of being embedded in or anchored to highly porous support materials. Fullerene C_{60} was used as PEI cross-linker to obtain a highly selective CO_2 sorbent, PEI-C_{60}, with high absorption capacity at low CO_2 partial pressures and relatively warm temperatures, low temperature of regeneration, and no corrosion issues. Specifically, PEI-C_{60} can absorb up to 0.17 g CO_2 per g of material already at 0.25 bar and 90 °C,[3-4] and be fully regenerated at the same temperature, significantly lower than that of amine solutions (120 °C). Apart from its notable properties, PEI-C_{60} has a major limitation, namely decreased CO_2 uptake at temperatures below 90 °C under dry conditions. The limited absorption capacity at lower temperatures in dry conditions is due to the small surface area of the material and the resulting limited gas diffusion in the bulk.[5] The latter is a commonly dominant limitation in highly loaded polyamines.[6-7]

Unfavourable uptake kinetics of highly loaded amino-polymer sorbents at ambient temperature has been extensively reported in previous studies. Several groups studied PEI and

observed higher CO_2 capture capacity with increasing temperature.[8-11] The specific behaviour was mainly attributed to improved diffusion and enhanced molecule flexibility.[6, 12] Mass transport limitations in highly loaded sorbents have also been examined in a recent study by Wilfong et al. using diffuse reflectance infrared Fourier transform spectroscopy (DRIFTS).[13] Tetraethylenepentamine (TEPA) films of three different thicknesses were analysed, revealing decreased amine efficiency (moles of captured CO_2 / moles of amine) with increasing film thickness due to the CO_2 diffusion hindrance in the bulk of the material. As revealed by DRIFTS analyses, surface ammonium carbamates formed upon CO_2 adsorption result in the creation of an electrostatically charged interconnected network hindering further CO_2 diffusion in the bulk.[13]

Opposite to metal organic frameworks (MOFs) where reduced CO_2 uptake is reported in the presence of water vapor,[14-16] enhanced CO_2 uptake and amine efficiency is experimentally observed for immobilized amines under humid conditions.[17-20] Some groups relate this remarkable enhancement to the plasticizing effect of water on the macromolecular chains affecting the semi-crystalline structure of the amino polymers.[21-22] Based on liquid amines chemistry, it is also suggested that the increase is caused by bicarbonate formation. This was recently demonstrated to happen after long CO_2 sorption times in materials with particularly low amine surface coverage, where infrared (IR) bands were detected and assigned to bicarbonate species after subtracting alkylammonium carbamate bands.[23] Low concentrations of bicarbonate was also observed by Foo et al.[24] who proposed its formation with primary, secondary, and tertiary amines. Nevertheless, the presence of large amounts of carbamates and carbamic acid renders the observation of bicarbonate difficult.[24] Likewise, Hahn et al.[25] identified bicarbonate species using ^{13}C NMR and on such basis explained the increased capture capacity in the presence of water vapor because of bicarbonate formation. The same

experimental technique was applied by Moore et al. to draw similar conclusions.[26] On the other hand, relevant FTIR studies investigating the type of adsorbed species dismissed bicarbonate formation in the past.[27] Yu and Chuang[28] linked the increase of CO_2 uptake to the loosening effect of water on the interactions between amine functionalities resulting in increased availability of amines for CO_2 capture under humid conditions. Alternatively, enhanced capture capacity in the presence of water vapor was associated to the release of additional amine groups via hydrolysis of silylpropylcarbamates according to Bacsik et al.[29] In a different study, Gebald et al.[30] observed an increase of CO_2 capture capacity under humid conditions, especially in ultra-diluted conditions, and proposed a water-enhanced accessibility effect on amines sites otherwise hindered in the bulk. In previous work Mebane et al.[31] developed a microstructural model where zwitterion diffusive intermediates govern the transport and resulting CO_2 capacity of highly loaded amine sorbents. Zwitterions stability under anhydrous conditions was called into question, as quantum chemistry studies showed that zwitterions could only be stable in polar environments such as that of water.[31] Nevertheless, in a more recent study the same group has verified that it is indeed the zwitterion to serve as a diffusive intermediate stabilized in the presence of water. Furthermore, it was shown that water-stabilized zwitterions had lower activation energy for conversion to product and outnumbered the amine-stabilised ones. Bicarbonate species were again disfavoured, suggesting the formation of hydronium carbamate instead.[32]

In this study, we searched for molecules alternative to water with an H_2O-like enhancing effect on the diffusion of CO_2 in highly loaded amine sorbents. The reason was to compare molecules alternative to water and identify the key features responsible for the enhanced CO_2 transport effect. We did this with an ideally suited material made from the cross-linking of PEI. The low surface area and resulting high diffusion limitations of this material, enabled us

to estimate the impact of diffusion hindrance on CO_2 capture and clearly identify molecules able to partner with CO_2 to overcome this barrier. Partner molecules were selected according to their Hansen solubility parameters values, targeting those with dispersive, polar, and hydrogen bonding values in various degrees similar to those of water.

Experimental methods

Materials. Polyethyleneimine branched (M_w = 25,000 Da, Aldrich), fullerene C_{60} (+99%, Sigma-Aldrich), toluene (99.9%, Sigma-Aldrich), $CHCl_3$ (+99.9%, Sigma-Aldrich), methanol (99.8+%, Acros Organics), ethanol absolute (99.8+%, Fischer Chemical), isopropanol (99.5+%, Acros Organics), triethylamine (99%, Acros Organics), $^{13}CO_2$ (99% ^{13}C, <3% ^{18}O, Sigma-Aldrich) and D_2O (99.9%, Cambridge Isotope Laboratories) were all used as received. Ar and CO_2 pure gases were supplied by BOC gases. Deionized water was available in-house.

PEI-C_{60} synthesis. In one vial 10 mg of C_{60} was dissolved in 12 mL of toluene, while in another vial 0.1 g of PEI was dissolved in 3 mL $CHCl_3$. 0.5 mL of Et_3N was added to the C_{60} solution to which the PEI was then added too. After shaking strongly, a brown precipitate was formed that was separated and washed with excess $CHCl_3$ on a PTFE filter (0.45 μm pores). Once dried, the solid product, PEI-C_{60}, appeared as a brown-red rubbery solid.

CO_2 uptakes. A TA Instruments SDT Q600 Thermogravimetric Analysis/ Differential Scanning. Calorimetry (TGA/DSC) was used for all gas uptakes. Capture tests were carried out at atmospheric pressure in the following sequence: i) activation to remove the pre-absorbed species at 90 °C under Ar flow, ii) initiation of gas uptake at 25 °C by flowing dry CO_2, H_2O-saturated Ar, H_2O-saturated CO_2, MeOH saturated Ar, MeOH saturated CO_2, EtOH saturated Ar, EtOH saturated CO_2, IPA saturated Ar, IPA saturated CO_2, $CHCl_3$ saturated Ar and $CHCl_3$ saturated CO_2. Solvent saturated or dry gases were prepared using a stainless-steel

bubbler filled either with H_2O, D_2O, MeOH, EtOH, IPA, $CHCl_3$ or dry molecular sieves respectively, iii) purging Ar at 25 °C to remove the weakly absorbed species and iv) temperature programmed desorption with a heating rate of 5 °C/min from 25-90 °C in Ar atmosphere. All the steps were performed until equilibration.

Pre-hydration tests. In the case of pre-hydrated PEI-C_{60} uptake tests, the procedure took place as follows: i) the sample was activated at 90 °C under Ar atmosphere, ii) the sorbent was equilibrated to a constant weight under humid Ar streams of different flowrates, i.e., 30, 50, and 80 mL/min resulting in gas streams of 19.7, 20.9 and 21.4 %RH respectively, iii) the material was subsequently exposed to humid CO_2 using the same flowrates as in hydration step. Desorption procedure remained the same as in *CO_2 uptakes*.

Infrared spectroscopy. A FTIR Nicolet Nexus 670 equipped with ATR Smart Golden Gate diamond crystal was used to collect the attenuated total reflectance infrared spectra of PEI-C_{60} prior and after conditioning. All samples were transferred from the TGA to the ATR-FTIR in vials filled with the same gas used for conditioning. Conditioning took place through a two-stage process. In the first stage, PEI-C_{60} was kept at 90 °C for 1h, while in the second stage the temperature was decreased to 25 °C in about 2 h and held at the same temperature for 3 h. The following gases were used for conditioning: CO_2, $^{13}CO_2$, H_2O-saturated Ar, D_2O-saturated Ar, H_2O-saturated CO_2, H_2O-saturated $^{13}CO_2$, D_2O saturated CO_2 and D_2O saturated $^{13}CO_2$.

Combined TGA-FTIR. Exhaust gases desorbed from the material were introduced to the FTIR Nicolet Nexus 670 apparatus equipped with a TGA-IR interface through a heated line (200 °C).

Results and discussion

Promoting effect of H_2O on CO_2 uptake

Previous studies from our group report that PEI-C_{60} can absorb up to 0.21 g/g of CO_2 at room temperature only in the presence of moisture, as a much lower uptake is achieved in dry conditions. Water appears to play a critical role in this process since the uptake in dry CO_2 is more than ten times smaller, barely approaching 0.018 g/g.[5] To better understand this finding we decided to investigate the effect of pre-hydration on the CO_2 capture performance of PEI-C_{60}. The material was hydrated to three different degrees (0.50, 0.60, and 0.68 g H_2O/g material) using humid Ar stream of different relative humidities (19.7 %, 20.9 % and 21.4%), and subsequently exposed the pre-hydrated materials to humid CO_2, all of this at a fixed temperature of 25 °C. As shown in Figure 1, higher water loadings lead to higher and faster CO_2 uptakes. In particular, with the largest water loading, 0.68 g/g, the resulting CO_2 uptake is 0.17 g/g, close to the maximum capture capacity of the material and corresponding to an amine efficiency of 0.21 (based on a weight ratio PEI:C_{60} = 78.8:21.2, as from reference 5). The uptakes after preloading 0.50 and 0.60 g/g of H_2O are 0.14 g/g and 0.16 g/g of CO_2 corresponding to an amine efficiency of 0.20 and 0.18 respectively. It is therefore clear that not only the presence of water is critical to the enhancing effect, but also the amount of it affects the resulting capture rate and capacity. This is further shown in Figure 2 where the CO_2 absorption rate in the prehydrated material is much higher compared to that measured in other experimental conditions. In the prehydrated material, full absorption is achieved in the first 2 minutes of exposure to CO_2 (black curve), while it takes up to 60 minutes to reach the same capture capacity starting from a dry sample and using a CO_2 wet stream at 90 °C (red curve). A measurable drop of the capture performance is observed when dry CO_2 is used at the same temperature (blue curve), deeply worsened if the temperature of absorption is brought down to 25 °C (green curve). It follows that water has a beneficial effect at both low and high temperature of absorption.

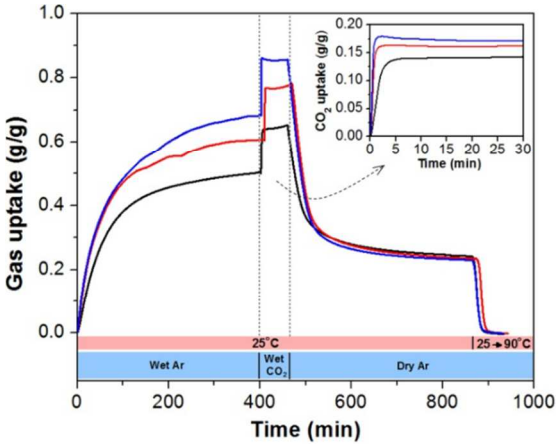

Figure 1. Effect of pre-hydration on the CO_2 capture performance of PEI-C_{60}. At 25 °C, the dry material was first hydrated using wet Ar at relative humidities of 19.7, 20.9 and 21.4 % reaching water loadings of 0.50, 0.60, and 0.68 g H_2O/g material, corresponding to the black, red, and blue curves, respectively. After hydration, the gas stream was switched to wet CO_2 and sharp CO_2 uptakes were recorded, also shown in the inset for ease of comparison. The gas flow was then switched to dry Ar and mass losses were observed due to the desorption of water and weakly sorbed CO_2. Residual masses were left in the samples accounting for about 0.23 g/g of strongly sorbed CO_2 hydrated species. These species could only be desorbed when the temperature was increased from 25 to 90 °C (5 °C/min), as shown in the ending part of the curves. All measurements were performed at atmospheric pressure.

In Figure 2, it is also interesting to note that the absorption curve of the pre-hydrated material goes through a maximum, probably due to a larger amount of water co-captured during fast CO_2 absorption and then slowly released as equilibrium is reached. As a matter of fact, most of the water present in the material can be easily desorbed in an Ar stream at 25 °C leaving just a small amount of it strongly absorbed in CO_2-H_2O species that can only be removed at 90 °C, as shown in Figure 1. It is intriguing to notice that the amount of strongly absorbed species is similar in all the examined cases, 0.23 g/g, independently of the quantity of pre-loaded water. This is related to the amount of strongly bounded CO_2, which is most likely the same in all cases and lower than the total amount of CO_2 present in the material when held in CO_2 environment. In other words, some of the captured CO_2 is absorbed in the form of weakly

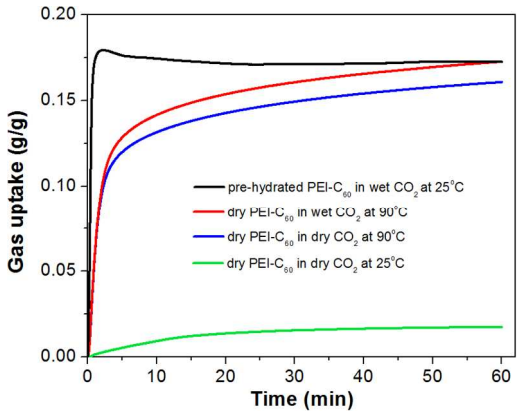

Figure 2. Comparison of CO_2 uptake performance of PEI-C_{60}. The dry material was exposed to dry CO_2 at 25 °C (green curve) or 90 °C (blue curve) with improved uptake at higher temperature. When the dry material was exposed to wet CO_2 (red curve) a further increase of mass was observed due to the formation of strongly bonded CO_2-H_2O species. When a pre-hydrated material was used, wet CO_2 was absorbed much faster (black curve) showing the extreme enhancing effect of water on the CO_2 capture rate of highly loaded amine sorbents.

bound species and can be desorbed when the material is simply exposed to Ar. This has been observed experimentally using FTIR, as reported later in this section. These weakly absorbed species are likely formed from water and carbamic acid.[28, 33]

In support of the observed enhancing effect of water, the rate of CO_2 absorption of pre-hydrated PEI-C_{60} was analysed using different kinetic models, details of the fittings are provided in the Supporting Information. CO_2 uptakes were best fitted using the modified Avrami kinetic model considered to be a correction for diffusion limitations to a first-order sorption process.[5] The values of the model parameters, i.e. kinetic constant k_a, absorption plateau w, and correction factor m, were extrapolated from the fittings of the CO_2 absorption curves shown in Figure 3. These values were then used to calculate the rates of CO_2 absorption reported in the corresponding inset. It is evident that as the amount of water pre-loaded in the sorbent increases, the rate of sorption also increases. In going from a pre-hydration level of 0.50 to 0.68 g H_2O per gram of material the rate of absorption quintuplicates. Such a significant increase of capture rate

(and capacity) with increasing water content is further evidence of the strong promoting effect of water towards CO_2 uptake in amine loaded sorbents.

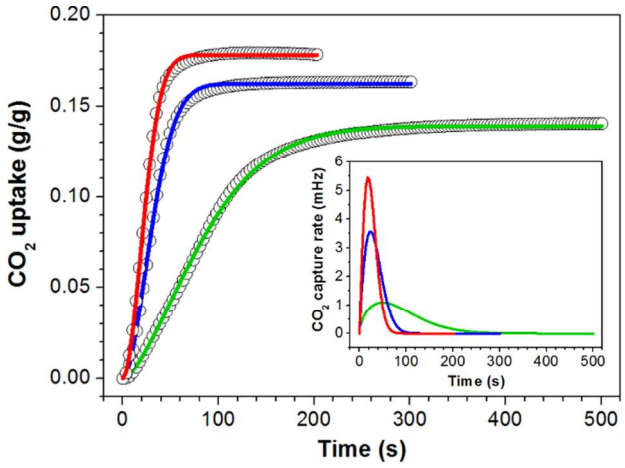

Figure 3. CO_2 uptake kinetic fittings and corresponding CO_2 absorption rates for pre-hydrated PEI-C_{60}. The experimental data of wet CO_2 capture (open circles) are taken from the inset of Figure 1 and are superimposed with their modified Avrami fittings for pre-hydration levels 0.50 g/g (green line), 0.60 g/g (blue line), and 0.68 g/g (red line). Being interested in comparing the initial rates of CO_2 absorption, only the first parts of the experimental curves have been considered. In the inset, a comparison of the CO_2 capture rates calculated from the first derivative of the modified Avrami fitting curves is shown. Clearly, the rate of absorption is greatly dependent on the pre-hydration level with faster kinetics in the presence of larger amounts of pre-loaded water.

To verify the formation of weakly sorbed CO_2-H_2O species upon wet CO_2 capture, PEI-C_{60} was exposed to a humid CO_2 stream followed by dry Ar while the desorbed species were monitored using tandem TGA-FTIR. The dry material was first saturated with water and CO_2 reaching an overall loading of about 0.42 g/g. This loading is taken as the first point of the gas desorption curve presented in Figure 4. As dry Ar was flowing, the mass of the sample dropped to a plateau at 0.21 g/g in agreement with the terminal desorption value of 0.23 g/g observed for all pre-hydrated samples presented in Figure 1. A relevant set of IR spectra of the desorbed gases

is presented in the inset of Figure 4, where the absorption bands associated to the asymmetric stretch and bending modes of CO_2 are observed at about 2350 and 675 cm^{-1}, respectively. The broad features at 4000-3500 cm^{-1} and 1750-1250 cm^{-1} are mostly due to the rotational fine structure of the three fundamental vibrational modes of water: the O-H symmetric and asymmetric stretching, and the H-O-H bending, respectively.

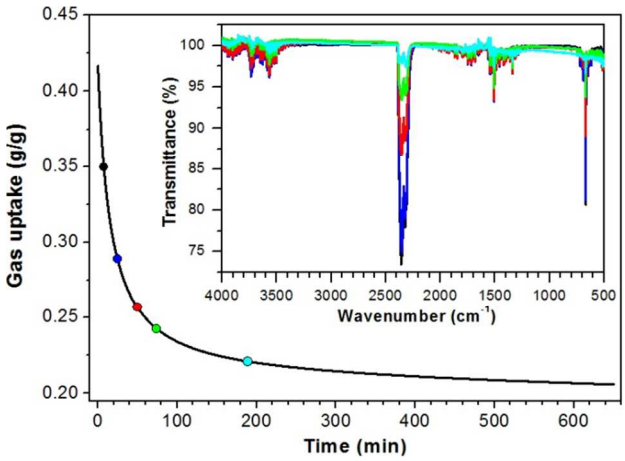

Figure 4. Identification of species desorbed from PEI-C_{60} after uptake. First, the material was exposed to wet CO_2 reaching an overall uptake of 0.42 g/g at 25 °C, which is the starting gas uptake value of the desorption curve presented in the main plot. The desorption was performed in dry Ar also at 25 °C until the residual uptake reached a plateau value of 0.21 g/g. The desorbed species were monitored using infrared spectroscopy, representative IR spectra are presented in the inset. The spectra were taken at the times indicated on the desorption curve with dots of the same color of their corresponding spectra.

Clearly, both CO_2 and H_2O were detected in the Ar stream carrying the gases desorbed from PEI-C_{60} at 25 °C. In particular, the asymmetric stretch band of CO_2 appears almost unchanged after about 7 and 15 min from the start of the desorption (black and blue spectra, respectively), dropping substantially only after 45 min (red spectrum), yet still desorbing in smaller amounts after 90 min (green spectrum). The modest temperature of desorption points to the formation of weakly bound CO_2-H_2O species, however unlikely to be simple adsorbed gas molecules given

the extended time needed for desorption. This supports our previous observations that apart from weakly absorbed water, carbamic acid can also be desorbed at ambient temperature.

IR evidence of hydrated carbamate species

FTIR-ATR spectra of PEI-C_{60} were collected after conditioning the material in different gaseous environments, the spectra are presented in Figure 5. $^{13}CO_2$ and D_2O were used to establish whether characteristic vibrational peaks of carbamate would show any isotopic effect upon using D_2O in place of H_2O. As presented in this section, spectral features assigned to carbamate species clearly shift to lower wavenumbers when deuterated water is used. This finding appears to support the formation of carbamate species where water is included in the local structure since the observed downshift should only be possible if water is involved in the corresponding vibrational modes. This adds important evidence to on-going work on the role of H_2O on CO_2 transport in the bulk of amine-loaded sorbent. To better appreciate this, it is useful to start from the assignment of the spectral features of PEI-C_{60} and examine the effect carbon capture and isotopic substitution on the spectra.

In Figure 5a, the IR spectra of as-received PEI (spectrum 1) and of PEI-C_{60} conditioned in dry Ar (spectrum 2) are almost identical. It follows that PEI does not undergo major chemical changes upon cross-linking with C_{60}. In Figure 5b, the spectral features of PEI-C_{60} are assigned to their respective vibrational modes. Starting from the left: the broad absorption peak above 3000 cm^{-1} is associated to the amine N-H stretching,[34] the two sharper peaks coming right after at 3000-2500 cm^{-1} are due to the methylene bridge C-H stretching,[35-36] the doublet centred at 1600 cm^{-1} to N-H deformation,[34] the single peak at 1450 cm^{-1} to the C-H scissoring,[34] and the last three doublets to C-H wagging, C-N stretching, and N-H bending at 1300, 1100, and 900 cm^{-1}, respectively.[34-36] The spectra can be normalised against the intensity of the C-H symmetric

stretching (2800 cm^{-1}) or scissoring (1450 cm^{-1}) to compare the changes in the high (4000-1800 cm^{-1}) or low (1800-700 cm^{-1}) wavenumber range, respectively. This choice of reference peaks is based on the expected limited effect of CO_2/$^{13}CO_2$ and/or H_2O/D_2O absorption on the vibrational modes of the methylene of PEI.

The effect of H_2O or D_2O on the infrared spectra of PEI-C_{60} is presented in Figure 5. In Figure 5c, a large increase of absorption due the additional O-H and N-H^+ stretching vibrations is observed above 3000 cm^{-1}.[36] In the case of D_2O, a second large band is also observed at about 2500 cm^{-1} due to the O-D stretching.[37] In Figures 5d, the absorption of water affects mainly two parts of the spectra. The first part at 1600 cm^{-1} is the peak of N-H^+ deformation, originally related the unprotonated N-H deformation,[36] shifting toward lower frequencies upon protonation or deuteration. This is also highlighted in Figure 6 where the relevant peaks are identified with asterisks. The second major change is the significant fading of the N-H bending absorption at 1000-800 cm^{-1}, likely caused by protonation/deuteration of the amine groups of PEI. Thus, the main effect of water absorption alone (no CO_2) is to protonate or deuterate the amine groups of the sorbent. A rather obvious finding, nonetheless important since the spectral changes due to water absorption in the presence of CO_2 can be then reasonably associated to the interaction of water with the carbamate species formed upon CO_2 capture.

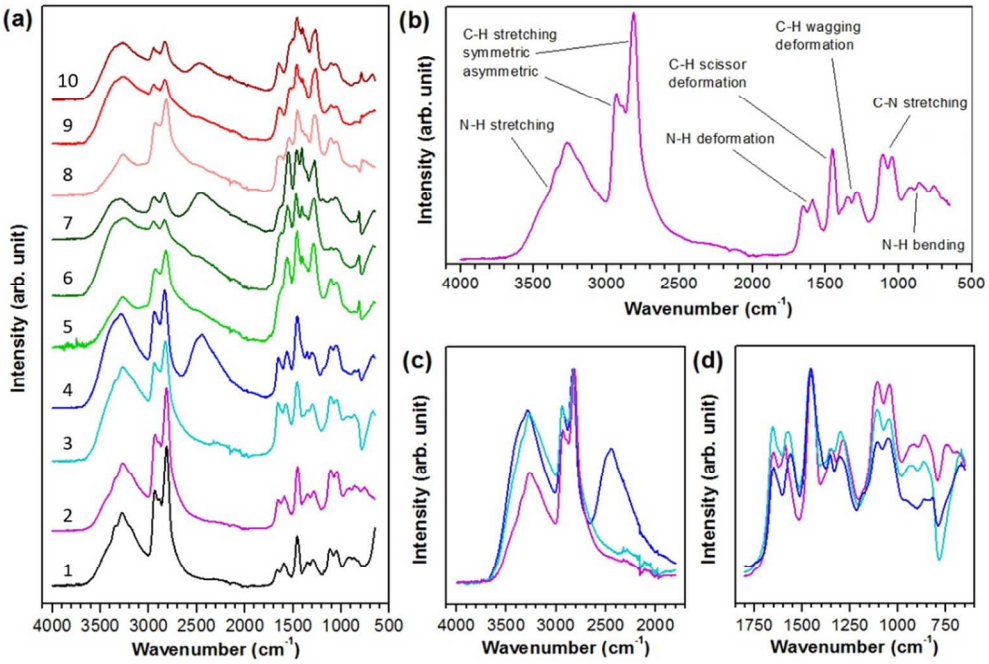

Figure 5. Infrared spectra of as-received PEI, and PEI-C_{60} conditioned in different gasses. (a) FTIR-ATR spectra of 1) as-received PEI, and PEI-C_{60} conditioned 2) dry Ar, 3) Ar-H_2O, 4) Ar-D_2O, 5) dry CO_2, 6) CO_2-H_2O, 7) CO_2-D_2O, 8) dry $^{13}CO_2$, 9) $^{13}CO_2$-H_2O, and 10) $^{13}CO_2$-D_2O. (b) Assignment of the absorption bands of PEI-C_{60} conditioned in dry Ar. (c) Comparison of the spectral features of PEI-C_{60} conditioned in dry Ar, H_2O-Ar, and D_2O-Ar, where spectra are normalised on the intensity of the C-H symmetric stretching peak at 2800 cm^{-1}; whereas in (d) spectra are normalised on the intensity of the C-H scissor deformation peak at 1450 cm^{-1}.

The absorption of CO_2 or $^{13}CO_2$ with or without H_2O or D_2O has been considered too, and all relevant infrared spectra are presented in Figure 5a (spectrum 3 to spectrum 10). As CO_2-H_2O (spectrum 6) or $^{13}CO_2$-H_2O (spectrum 9) are absorbed into PEI-C_{60}, the C-H stretching peaks centred at 2800 cm^{-1} are almost overtaken by a very broad and intense absorption band spanning from 2000 to 3000 cm^{-1}. Similar changes are observed in the case of CO_2-D_2O (spectrum 7) or $^{13}CO_2$-D_2O (spectrum 10). One major cause of this broadening is the effect of hydrogen bonding between ammonium ($R\text{-}NH_3^+$/$R_1R_2\text{-}NH_2^+$) and carbamate ($-NCOO^-$) on the N-H stretching of ammonium carbamate species.[38] Infrared absorption peaks

due to carbamate species are also found in the low wavenumber region, as shown in the spectra regrouped in Figure 6. Here, two main peaks associated to carbamate species are found at about 1560 cm^{-1}, for the COO^- stretching, and at about 1290 cm^{-1}, for the $NCOO^-$ skeletal vibration.[13] The spectra of PEI-C_{60} conditioned in dry Ar, dry CO_2, and dry $^{13}CO_2$ are compared in Group I. As CO_2 is absorbed, a peak for carbamate COO^- stretching is evident at 1562 cm^{-1}, this peak shifts to 1538 cm^{-1} when $^{13}CO_2$ is used instead. This corresponds to a downshift of 24 cm^{-1} comparable to the 28 cm^{-1} measured for the same isotopic substitution reported for the COO^- asymmetric stretch of carbamate zwitterion ($NH_3^+COO^-$).[39] Accordingly, the peak of $NCOO^-$ skeletal vibration at 1290 cm^{-1} downshifts of 14 cm^{-1}, confirming that both peaks are related to carbon dioxide. Peaks of lower intensity not affected by the isotopic substitution appear at about 1400 cm^{-1}. These are assigned to the bending vibrations of ammonium formed from the transfer of protons from carbamic acid to amine functions.[38]

The infrared spectra of PEI-C_{60} conditioned in wet Ar, CO_2-H_2O, and $^{13}CO_2$-H_2O are compared in Group II of Figure 6. The isotopic shifts of the peaks associated to carbamate are either larger (COO^- stretching) or comparable ($NCOO^-$ skeletal vibration) to those observed in Group I for dry CO_2 absorption. Moreover, the ammonium peaks in Group II are more pronounced because of further amine protonation in the presence of water. Similar changes are observed for Group III, where D_2O is used in place of H_2O. Most importantly, the isotopic shifts between Groups II and III are evidence of the interaction of water with the carbamate moieties, as discussed at the beginning of this section. From a comparison of spectra of PEI-C_{60} conditioned in CO_2-H_2O (Group II) and CO_2-D_2O (Group III), it is evident that the peak of carbamate at 1560 cm^{-1} downshifts when deuterated water is used. This effect is also evident in going from $^{13}CO_2$-H_2O (Group II) to $^{13}CO_2$-D_2O (Group III). It follows that water is

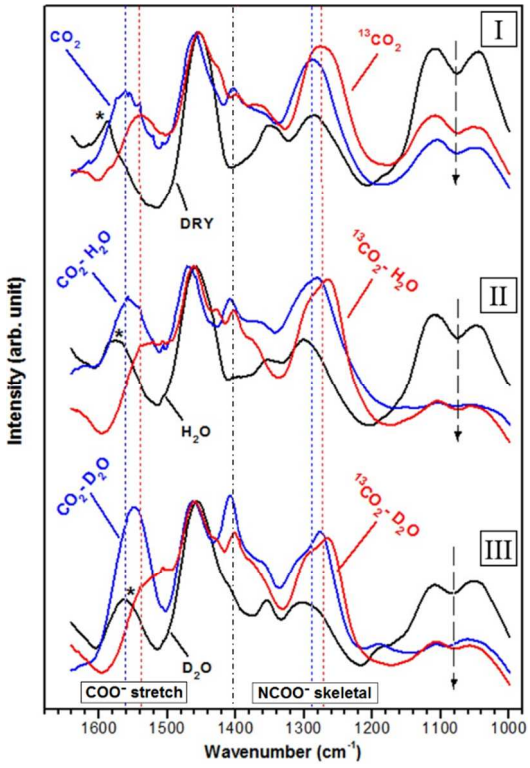

Figure 6. Isotopic shifts and band intensity changes observed in the infrared spectra of PEI-C_{60}. Spectra are organised in three groups: I, II, and III. Group I: PEI-C_{60} conditioned in dry Ar, dry CO_2, and dry $^{13}CO_2$. Group II: PEI-C_{60} conditioned in Ar-H_2O, CO_2-H_2O, and $^{13}CO_2$-H_2O. Group III: PEI-C_{60} conditioned in Ar-D_2O, CO_2-D_2O, and $^{13}CO_2$-D_2O. All groups normalised to the intensity of the C-H scissor deformation peak at 1450 cm^{-1}. The red and blue dashed lines indicate the isotopic shifts of two distinct absorption features (COO^- stretch and $NCOO^-$ skeletal vibration) due to the carbamate species formed upon carbon capture. The black dash-dotted line shows the peaks related to the bending of ammonium groups. The asterisks on the left-hand-side show the isotopic shift of the N-H deformation peak due to protonation or deuteration as H_2O or D_2O is absorbed, respectively. The arrows on the right-hand-side highlight the significant drop of intensity of the C-N stretching band of PEI as carbon dioxide is captured.

involved in the vibrational modes on the carbamate moieties since these shifts can only be observed if atoms partaking in the vibration are isotopically substituted. This finding is particularly relevant considering the facilitating role of water on CO_2 capture. Currently,

theoretical and experimental evidence support the hypothesis that zwitterions intermediates (amine^{+}-CO_2^{-}) enhance CO_2 transport in PEI.[31-32] These intermediates can be stabilised in the presence of water (amine^{+}-CO_2^{-}···H_2O), and from our findings it appears that water is eventually integral part of the resulting carbamate species, possibly in the form of hydronium carbamate (with structure amine-CO_2H···OH_2, as proposed by Mebane et al.[32]). A last notable change in the IR spectra of PEI-C_{60} is the drop of intensity of the C-N stretching band at about 800-1200 cm^{-1} upon CO_2 absorption, shown with dashed arrows in Figure 6. This is evident in all Groups, I, II, and III, especially in wet conditions. A possible explanation for this is a reduced mobility of the PEI chains[40] because of the strong ionic interactions acting among hydrated ammonium carbamate moieties. This induced rigidity could be the reason of the limited amine efficiency of PEI-based materials[41] usually between 0.2-0.3 mol of CO_2/mol of amine, considerably lower than theoretical value of 0.5 in the case of ammonium carbamate formation.

Effect of partner molecules on CO_2 uptake

The results presented in the previous sections demonstrate that water has a strong promoting effect on the CO_2 capture rate and capacity of PEI-C_{60} at ambient temperature. This effect has been observed in many other PEI-loaded materials[17-18, 20, 22] where water and CO_2 are supposed to form diffusive intermediates responsible for CO_2 transport in PEI.[31-32] If water is not present, this facilitated transport is not possible and the CO_2 absorption performance of PEI at room temperature is poor. Moreover, our infrared studies indicate a direct participation of H_2O in the chemical environment of the carbamate moieties formed upon absorption of wet CO_2. Intrigued by these facts, we decided to search for other "partner molecules" able to facilitate CO_2 transport in PEI, and from a comparison of these molecules identify the key features responsible for such a promoting effect. To this end, we investigated the absorption of CO_2 in the presence of methanol

(MeOH), ethanol (EtOH), isopropyl alcohol (IPA), and chloroform ($CHCl_3$). In practice this was done by using a stream of CO_2 bubbled through each different solvent (one at the time), in the same way CO_2 was bubbled through water for wet CO_2 absorption. We targeted these molecules based on the increasing difference of the values of their Hansen Solubility Parameter (HSPs) from those of water, as reported in Table 1. HSPs describe the interaction of a solvent molecule with others of its kind.[42] This interaction results from the combination of three contributions: London dispersion forces (δ_D), permanent dipole-permanent dipole polar forces (δ_P), and hydrogen bonding forces (δ_H). The total cohesion energy (E) of the solvent can be calculated from these three parameters since $(E/V)^2 = \delta_D^2 + \delta_P^2 + \delta_H^2$, where V is the molar volume of the solvent.[42] As can be seen in Figure 7, among the different solvents δ_D is about constant, whereas δ_P and δ_H clearly decrease. In particular, a large drop of hydrogen bonding is evident in going from water to methanol. Instead, the polar contribution δ_P decreases regularly across the different solvents with chloroform the less polar among all. These are important changes since they affect the CO_2 transport capabilities of the partner molecules in PEI, as discussed in the following.

Table 1. Hansen Solubility Parameters Values for the Listed Solvents

Solvent	δ_D ($MPa^{1/2}$)	δ_P ($MPa^{1/2}$)	δ_H ($MPa^{1/2}$)
Water	15.5	16.0	42.3
Methanol	15.1	12.3	22.3
Ethanol	15.8	8.8	19.4
Isopropanol	15.8	6.1	16.4
Chloroform	17.8	3.1	5.7

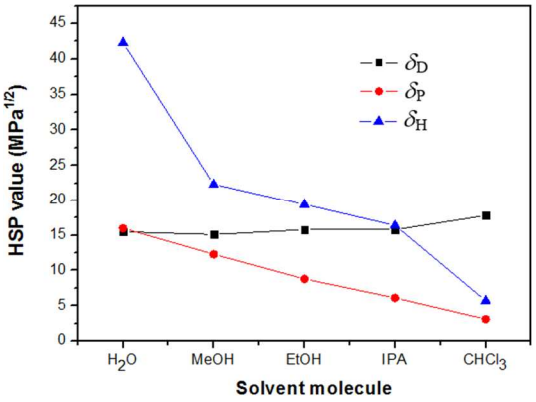

Figure 7. Trend of Hansen solubility parameters values for the solvents tested as partner molecules of CO_2 transport in PEI-C_{60}. Dispersive, polar, and hydrogen bonding contributions are shown as δ_D, δ_P, and δ_H, respectively.

The uptakes of solvent molecules in Ar or CO_2 stream are presented in Figure 8. The flow rate was fixed at 80ml/min for both gases, all mass uptakes were measured at 25 °C and atmospheric pressure. In Figure 8a, it is evident that PEI-C_{60} can absorb a significant amount of each solvent when Ar is used. The actual amount is dependent on (i) how much solvent is carried to the sample by the gas stream and (ii) the affinity of the material towards the solvent molecules. It is beyond the aim of the study to examine the difference in solvent uptake in Ar, while it is essential to compare the change in solvent uptake when CO_2 is used in place of Ar. For this reason, it is necessary to compare Figures 8a and 8b. Strikingly, PEI-C_{60} can absorb 0.27 g/g of $CHCl_3$ when the solvent is carried in Ar, but practically no chloroform is absorbed when CO_2 is used instead. As shown in the inset of Figure 8b, the plateau of the CO_2-$CHCl_3$ sorption curve (light blue solid line) is only slightly above that of dry CO_2 (black dotted line) meaning that even in the presence of $CHCl_3$ most of the captured mass is CO_2. A possible explanation of this is the formation of carbamate species upon CO_2 capture. These electrically charged species prevent $CHCl_3$

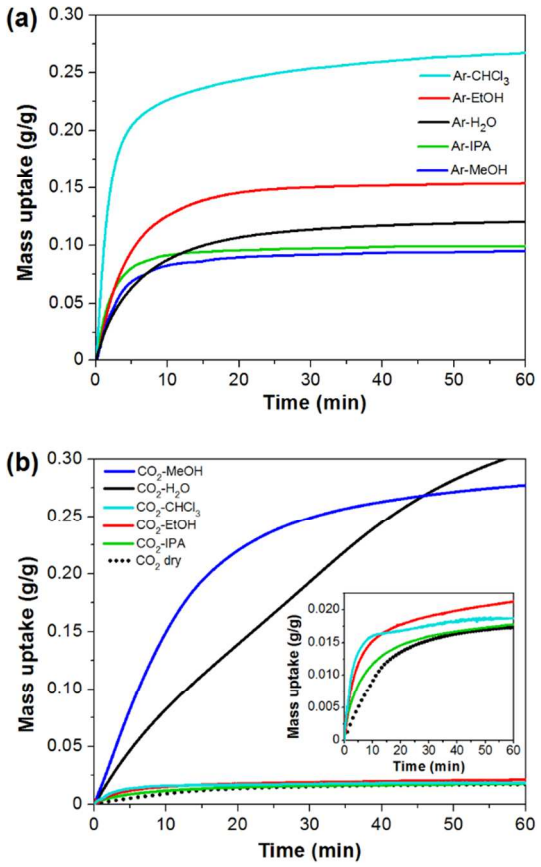

Figure 8. Mass uptakes of (a) solvent molecules carried in Ar stream and (b) solvent molecules and CO_2 transported in carbon dioxide stream for dry PEI-C_{60} at 25 °C. Also in (b), the uptake of dry CO_2 is included for comparison purposes, while the inset is an enlargement of the lower uptake curves. In all cases the same value of gas flow rate of 80 ml/min was used.

molecules from entering in the PEI and only a small amount of solvent is absorbed (~ 1 mg/g). This was confirmed experimentally using PEI-C_{60} first exposed to dry CO_2, once CO_2 is present in the material chloroform couldn't be absorbed from an Ar-$CHCl_3$ stream either. Similar results were obtained for EtOH and IPA (Figure S1). In Figure 8b, none or a very small amount of these solvents is absorbed when the carrier gas is CO_2. It follows that EtOH, IPA, and $CHCl_3$ do not have the required characteristics to enhance CO_2 transport in PEI-loaded sorbents. In other words, we can say that these molecules are unable to partner with CO_2 and form effective

diffusive intermediates required to enhance CO_2 capture at room temperature.

Methanol, like water, can enhance CO_2 transport in PEI at room temperature. When PEI-C_{60} was exposed to a CO_2-MeOH stream, the uptake of CO_2 and solvent reached about 0.27 g/g after 60 min exposure (blue solid line in Figure 8b). Also, the mass uptake was faster in the presence of MeOH than with H_2O (black solid line). Thus, MeOH and H_2O are both effective CO_2 partner molecules able to facilitate uptake in an otherwise diffusionally hindered PEI medium. A detailed comparison of absorption and desorption of CO_2 in the presence of H_2O or MeOH is presented in Figure 9. In Figure 9a, the mass of PEI-C_{60} increases when exposed to CO_2-H_2O or CO_2-MeOH at 25 °C reaching uptakes of about 0.4 and 0.3 g/g, respectively, in the first 400 min. As the gas is switched to dry Ar, the masses of loaded sorbents drop to about 0.2 g/g, a value comparable for both H_2O and MeOH-facilitated absorptions. These masses correspond to strongly bound CO_2 and solvent molecules that cannot be desorbed at 25 °C since they can only be released when the temperature is increased to 90 °C, as shown in the last part of the curves. Tandem TGA-FTIR was used to confirm the presence of solvent molecules in the strongly bound species. In the case of CO_2-H_2O, the mass of the sample decreased progressively as the temperature was increased to 90 °C (Figure 9b) and both CO_2 and H_2O were detected in the stream of desorbed gases (Figure 9c). In particular, the inset of Figure 9c shows that the infrared stretching features of water were detected during the all desorption stage, as from the green, red, and light blue IR spectra corresponding the dots placed on the desorption curve of Figure 9b. Infrared features of CO_2 were also detected with the strong absorption band at 2300-2400 cm^{-1} due to the asymmetric stretch of CO_2. Comparable results were obtained for CO_2-MeOH desorption. In Figure 9e, it is evident that both CO_2 and MeOH desorbed

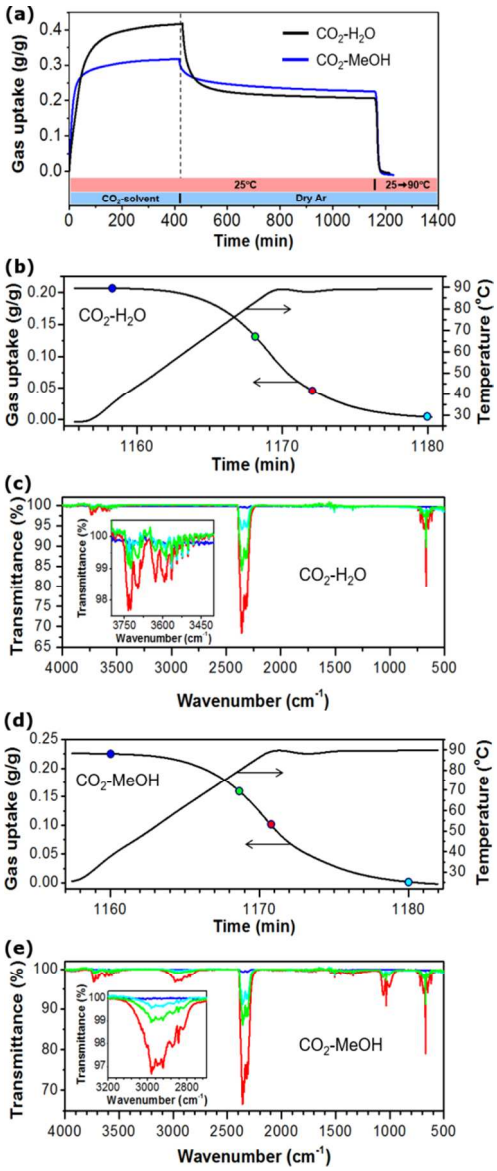

Figure 9. Absorption and desorption of CO_2-solvent gas mixtures on PEI-C_{60}. (a) Gas uptake of dry PEI-C_{60} exposed to CO_2-H_2O (black line) or CO_2-MeOH (blue line) at 25 °C, followed by desorption in dry Ar at 25 °C and then up to 90 °C. (b) Ending portion of the desorption curve of CO_2-H_2O as temperature is increased from 25 to 90 °C. Desorbed gasses were monitored using FTIR. (c) Representative infrared spectra demonstrate the release of both CO_2 and H_2O during heating. Spectra are of the same colour of the dots highlighted on the desorption curve in (b) showing the time they were taken. (d) Desorption of CO_2-MeOH during heating from 25 to 90 °C, and (e) related spectra with infrared abortion peaks of both CO_2 and MeOH. Spectra are colour-coded as the dots shown on the desorption curve in (d).

from the sample as the temperature was increased to 90 °C. The infrared absorption associated to the C-H bonds stretching of MeOH is highlighted in the inset of Figure 9e. Clearly, methanol was still detected in the gas stream even in the last part of the desorption curve, as from the infrared features of the light blue IR spectrum. This is a very significant finding since MeOH molecules required thermal energy (90 °C) to be desorbed together with CO_2 evidence of methanol being involved in interactions with carbamate species similarly to what observed in the case of H_2O.

Simplified structures of possible diffusive intermediates involving solvent-amine-CO_2 are presented in Figure 10. These structures are based on the physically bonded moieties proposed by Mebane et al.[31] where water interacts directly with the amine group in linear or ring topology, as shown in Figure 10a or 10b, respectively. Although the same authors reported that the activation energy barrier for carbamate formation from these structures is too high to explain experimental results (up to 300 kJ/mol), [32] we find relevant considering them anyway since solvent facilitate transport of CO_2 in PEI is presented for the first time in this study, and alternative pathways for carbamate formation might be conceived for partner molecules other than water. An immediate finding is that for partner molecules different than water the linear topology (Figure 10a) is not feasible because of a missing second O-H bond in MeOH, EtOH, and IPA required to interact with CO_2. The ring topologies for MeOH, EtOH, and IPA facilitated transport are presented in Figure 10c, d, and e, respectively. Clearly, the increased hindrance of the methyl, ethyl, and isopropyl groups make the ring more difficult to form. However speculative, this finding is in agreement with the experimental results presented here where MeOH is the only of these three molecules able to partner with CO_2 and facilitate transport in PEI. In Figure 10f, chloroform is even less predisposed to the

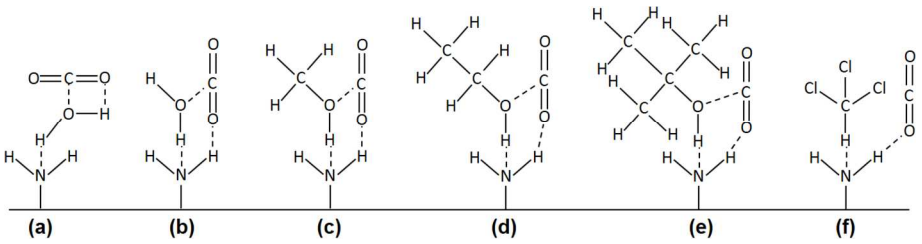

Figure 10. Simplified structures of possible diffusive intermediates involving a solvent molecule, a primary amine group of PEI, and a CO_2 molecule. When water is used, two structures are possible (a) linear or (b) ring topology.[31] The other ring topologies are for (c) MeOH, (d) EtOH, (e) IPA, and (f) $CHCl_3$. The dashed lines represent physical interactions among molecules responsible for the stability of the diffusive intermediates.

formation of a diffusive intermediate following either the linear or ring topology because of the lack of OH group, hence no CO_2 capture enhancement is observed when $CHCl_3$ is used in the place of water.

Another proposed diffusive intermediate is a water-stabilized zwitterion (H_2O-Zw),[32] as shown in Figure 11 for R = H. The H_2O-Zw (a) goes through a six-membered ring transition state (b) where water actively participate to the proton transfer to give the final captured species, a hydronium carbamate (c). In principle, the structure of an analogous transition state can be drawn for MeOH, EtOH, and IPA in (d) where R = $-CH_3$, $-CH_2CH_3$, and $-C(CH_3)_3$, respectively ($CHCl_3$ is excluded from this list since its central carbon does not have the non-bonding lone electron pairs of the hydroxyl oxygen necessary to allow for the proton transfer). It follows that the bulkiness of the substituent R group is likely to play again a crucial role in the stability and mobility of the diffusive intermediates. Also, the larger R is the more difficult the formation of the six-membered ring transition state should be, impeding in this way the conversion to the final hydronium carbamate. This agrees with the experimental finding of this study, where only MeOH with a small methyl substituent group is an effective partner molecule for CO_2 transport in PEI.

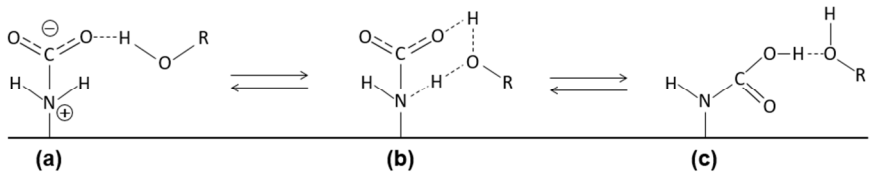

Figure 11. Simplified schematic showing the conversion of a CO_2 diffusive intermediate. The diffusive intermediate is (a) a solvent-stabilised zwitterion which goes through (b) a six-membered ring transition state to give (c) a hydronium carbamate, as proposed in reference 32. The group R represents either H, -CH_3, -CH_2CH_3, or -$C(CH_3)_3$.

The partner molecule steric hindrance is an important parameter to consider in explaining the very different enhancing transport effect of alcohols compared to water. However, these solvent molecules have in common a hydrogen bonding capability essential for the formation of any of the intermediate species shown in Figures 10 and 11. As previously mentioned, the extent of hydrogen bonding of solvents can be quantified and compared using the HSP δ_H. In Table 1, water has the highest δ_H, 42.3 $MPa^{1/2}$, while the value drops to almost half in the case of MeOH, 22.3 $MPa^{1/2}$. It is important to notice that despite such a significant drop of hydrogen bonding ability, MeOH is still an excellent CO_2 transport partner molecule with performance analogous to water (Figure 9a). On the other hand, when going from MeOH to EtOH the δ_H value decreases much less to 19.4 $MPa^{1/2}$, but EtOH does not enhance CO_2 transport (Figure 7). This suggests that while hydrogen bonding is required for a partner molecule to form diffusive intermediates, it is not as critical as would be expected since the extent of loss of hydrogen bonding capability does not directly correlate with a loss of CO_2 facilitated transport in PEI, as in the case of H_2O and MeOH. It follows that there must be other factors affecting the CO_2 capture enhancing effect of partner molecules. Besides δ_H, solvent molecules are characterised by other two HSPs, δ_D and δ_P, whose values are plotted in Figure 7. Cleary, δ_D is practically constant among the different

solvents, while δ_P decreases progressively in going from water to chloroform. The polarity of the solvent, represented by δ_P, appears then to be the other critical factor in enhancing the CO_2 transport in PEI together with hindrance since the London dispersive forces, represented by δ_D, are comparable among all solvents considered in this study. While extrapolated from a simple comparison of HSPs, this conclusion is in excellent agreement with the statement by Mebane et al. "that zwitterions are only stable – at least for certain chemistries – in a polar environment similar to that of water.[31] Thus, polarity and steric hindrance emerge as major factors in determining whether a solvent molecule can effectively partner with CO_2 to form zwitterionic diffusive intermediates and enhance carbon capture in highly loaded PEI sorbent materials at room temperature.

Conclusions

We report experimental evidence of the enhancing effect of methanol on the sorption performance of PEI-based CO_2 capture materials. While the enhancing effect of water has previously been reported, and further confirmed in this work, this is the first time that molecules alternative to H_2O are considered for their ability to facilitate CO_2 transport in PEI. Tandem TGA-FTIR studies demonstrate that MeOH not only enhances the diffusion of CO_2 in the bulk of PEI-C_{60} at room temperature, but also remains strongly bound to the material upon CO_2 capture. Evidently, both MeOH and H_2O have the appropriate molecular characteristics to form diffusive intermediates with CO_2 and the final absorbed products; for this reason, we refer to these molecules as effective CO_2 capture partner molecules. Other molecules have also been considered, but none among ethanol, isopropanol, and chloroform showed a significant carbon capture facilitating effect. A simplified comparison of possible diffusive intermediates structures and of Hansen solubility parameters for all these solvent molecules suggests that polarity and

steric hindrance play a major role in the enhancing effect. We hope other groups will follow up to these findings with studies of the mode of operation of MeOH on CO_2 transport in comparison to H_2O. Other partner molecules could also be found providing a wider range of diffusive intermediates from which to build a better understanding of the available mechanisms for improved CO_2 capture in PEI-loaded sorbent materials.

Supporting information

Tables S1-S3. CO_2 uptake fitting results for PEI-C_{60} hydrated to different degrees; Figure S1. Solvent uptake after CO_2 absorption at room temperature. This information is available free of charge via the Internet at http://pubs.acs.org

Acknowledgements

Financial support was provided by the Welsh Government through the Sêr Cymru Programme. This work is part of the FLEXIS (Flexible Integrated Energy Systems) research operation, which is part-funded by the European Regional Development Fund (ERDF), through the Welsh Government. The authors declare no competing financial interest.

References

1. *UK Climate Action Following the Paris Agreement*; Committee on Climate Change. 2016. https://www.theccc.org.uk/wp-content/uploads/2016/10/UK-climate-action-following-the-Paris-Agreement-Committee-on-Climate-Change-October-2016.pdf
2. Covert, T.; Greenstone, M.; Knittel, C. R., Will We Ever Stop Using Fossil Fuels? *J. Econ. Perspect.* **2016**, *30*, 117-138.
3. Andreoli, E.; Barron, A. R., Activation Effect of Fullerene C_{60} on the Carbon Dioxide Absorption Performance of Amine-Rich Polypropylenimine Dendrimers. *ChemSusChem* **2015**, *8*, 2635-2644.
4. Andreoli, E.; Dillon, E. P.; Cullum, L.; Alemany, L. B.; Barron, A. R., Cross-Linking Amine-Rich Compounds into High Performing Selective CO_2 Absorbents. *Sci. Rep.* **2014**, *4*, 7304.
5. Andreoli, E.; Cullum, L.; Barron, A. R., Carbon Dioxide Absorption by Polyethylenimine-Functionalized Nanocarbons: A Kinetic Study. *Ind. Eng. Chem. Res.* **2015**, *54*, 878-889.
6. Bollini, P.; Brunelli, N. A.; Didas, S. A.; Jones, C. W., Dynamics of CO_2 Adsorption on Amine Adsorbents. 2. Insights into Adsorbent Design. *Ind. Eng. Chem. Res.* **2012**, *51*, 15153-15162.
7. Cogswell, C. F.; Jiang, H.; Ramberger, J.; Accetta, D.; Willey, R. J.; Choi, S., Effect of Pore Structure on CO_2 Adsorption Characteristics of Aminopolymer Impregnated MCM-36. *Langmuir* **2015**, *31*, 4534-4541.
8. Son, W.-J.; Choi, J.-S.; Ahn, W.-S., Adsorptive Removal of Carbon Dioxide Using Polyethyleneimine-Loaded Mesoporous Silica Materials. *Microporous Mesoporous Mater.* **2008**, *113*, 31-40.
9. Ma, X.; Wang, X.; Song, C., "Molecular Basket" Sorbents for Separation of CO_2 and H_2S from Various Gas Streams. *J. Am. Chem. Soc.* **2009**, *131*, 5777-5783.
10. Chen, C.; Yang, S. T.; Ahn, W. S.; Ryoo, R., Amine-Impregnated Silica Monolith with a Hierarchical Pore

Structure: Enhancement of CO_2 Capture Capacity. *Chem. Commun.* **2009**, 3627-3629.
11. Serna-Guerrero, R.; Sayari, A., Modeling Adsorption of CO_2 on Amine-Functionalized Mesoporous Silica. 2: Kinetics and Breakthrough Curves. *Chem. Eng. J* **2010**, *161*, 182-190.
12. Xiaoxing Wang, V. S., Jason C. Clark,Xiaoliang Ma, Steven H. Overbury,; Song, X. X. a. C., Infrared Study of CO_2 Sorption over "Molecular Basket" Sorbent Consisting of Polyethylenimine-Modified Mesoporous Molecular Sieve. *J. Phys. Chem. C* **2009**, *113*, 7260-7268.
13. Wilfong, W. C.; Srikanth, C. S.; Chuang, S. S., In Situ ATR and DRIFTS Studies of the Nature of Adsorbed CO_2 on Tetraethylenepentamine Films. *ACS Appl. Mater. Interfaces* **2014**, *6*, 13617-13626.
14. Liang, Z.; Marshall, M.; Chaffee, A. L., Co_2 Adsorption-Based Separation by Metal Organic Framework (Cu-Btc) Versus Zeolite (13x). *Energy Fuels* **2009**, *23*, 2785-2789.
15. Schoenecker, P. M.; Carson, C. G.; Jasuja, H.; Flemming, C. J. J.; Walton, K. S., Effect of Water Adsorption on Retention of Structure and Surface Area of Metal–Organic Frameworks. *Ind. Eng. Chem. Res.* **2012**, *51*, 6513-6519.
16. Xian, S.; Peng, J.; Zhang, Z.; Xia, Q.; Wang, H.; Li, Z., Highly Enhanced and Weakened Adsorption Properties of Two MOFs by Water Vapor for Separation of CO_2/CH_4 and CO_2/N_2 Binary Mixtures. *Chem. Eng. J* **2015**, *270*, 385-392.
17. Zhang, H.; Goeppert, A.; Olah, G. A.; Prakash, G. K. S., Remarkable Effect of Moisture on the CO_2 Adsorption of Nano-Silica Supported Linear and Branched Polyethylenimine. *J. CO_2. Util.* **2017**, *19*, 91-99.
18. Zhang, L.; Zhan, N.; Jin, Q.; Liu, H.; Hu, J., Impregnation of Polyethylenimine in Mesoporous Multilamellar Silica Vesicles for CO_2 Capture: A Kinetic Study. *Ind. Eng. Chem. Res.* **2016**, *55*, 5885-5891.
19. Su, F.; Lu, C.; Chen, H. S., Adsorption, Desorption, and Thermodynamic Studies of CO_2 with High-Amine-Loaded Multiwalled Carbon Nanotubes. *Langmuir* **2011**, *27*, 8090-8098.
20. Qi, G.; Fu, L.; Giannelis, E. P., Sponges with Covalently Tethered Amines for High-Efficiency Carbon Capture. *Nat. Commun.* **2014**, *5*, 5796.
21. Fan, Y.; Labreche, Y.; Lively, R. P.; Jones, C. W.; Koros, W. J., Dynamic CO_2 Adsorption Performance of Internally Cooled Silica-Supported Poly(Ethylenimine) Hollow Fiber Sorbents. *AIChE Journal* **2014**, *60*, 3878-3887.
22. Tsoufis, T.; Katsaros, F.; Sideratou, Z.; Kooi, B. J.; Karakassides, M. A.; Siozios, A., Intercalation Study of Low-Molecular-Weight Hyperbranched Polyethyleneimine into Graphite Oxide. *Chem. Eur. J.* **2014**, *20*, 8129-8137.
23. Didas, S. A.; Sakwa-Novak, M. A.; Foo, G. S.; Sievers, C.; Jones, C. W., Effect of Amine Surface Coverage on the Co-Adsorption of CO_2 and Water: Spectral Deconvolution of Adsorbed Species. *J. Phys. Chem. Lett.* **2014**, *5*, 4194-4200.
24. Foo, G. S.; Lee, J. J.; Chen, C.-H.; Hayes, S. E.; Sievers, C.; Jones, C. W., Elucidation of Surface Species through in Situ FTIR Spectroscopy of Carbon Dioxide Adsorption on Amine-Grafted SBA-15. *ChemSusChem* **2017**, *10*, 266-276.
25. Hahn, M. W.; Steib, M.; Jentys, A.; Lercher, J. A., Mechanism and Kinetics of CO_2 Adsorption on Surface Bonded Amines. *J. Phys. Chem. C* **2015**, *119*, 4126-4135.
26. Moore, J. K.; Sakwa-Novak, M. A.; Chaikittisilp, W.; Mehta, A. K.; Conradi, M. S.; Jones, C. W.; Hayes, S. E., Characterization of a Mixture of CO_2 Adsorption Products in Hyperbranched Aminosilica Adsorbents by ^{13}C Solid-State NMR. *Environ. Sci. Technol.* **2015**, *49*, 13684-13691.
27. Danon, A.; Stair, P. C.; Weitz, E., FTIR Study of CO_2 Adsorption on Amine-Grafted SBA-15: Elucidation of Adsorbed Species. *J. Phys. Chem. C* **2011**, *115*, 11540-11549.
28. Yu, J.; Chuang, S. S. C., The Structure of Adsorbed Species on Immobilized Amines in CO_2 Capture: An in Situ IR Study. *Energy Fuels* **2016**, *30*, 7579-7587.
29. Bacsik, Z.; Ahlsten, N.; Ziadi, A.; Zhao, G.; Garcia-Bennett, A. E.; Martin-Matute, B.; Hedin, N., Mechanisms and Kinetics for Sorption of CO_2 on Bicontinuous Mesoporous Silica Modified with N-Propylamine. *Langmuir* **2011**, *27*, 11118-11128.
30. Gebald, C.; Wurzbacher, J. A.; Borgschulte, A.; Zimmermann, T.; Steinfeld, A., Single-Component and Binary CO_2 and H_2O Adsorption of Amine-Functionalized Cellulose. *Environ. Sci. Technol.* **2014**, *48*, 2497-2504.
31. Mebane, D. S.; Kress, J. D.; Storlie, C. B.; Fauth, D. J.; Gray, M. L.; Li, K., Transport, Zwitterions, and the Role of Water for CO_2 Adsorption in Mesoporous Silica-Supported Amine Sorbents. *J. Phys. Chem. C* **2013**, *117*, 26617-26627.
32. Li, K.; Kress, J. D.; Mebane, D. S., The Mechanism of CO_2 Adsorption under Dry and Humid Conditions in Mesoporous Silica-Supported Amine Sorbents. *J. Phys. Chem. C* **2016**, *120*, 23683-23691.
33. Mafra, L.; Cendak, T.; Schneider, S.; Wiper, P. V.; Pires, J.; Gomes, J. R.; Pinto, M. L., Structure of Chemisorbed CO_2 Species in Amine-Functionalized Mesoporous Silicas Studied by Solid-State NMR and Computer

Modeling. *J. Am. Chem. Soc.* **2017**, *139*, 389-408.
34. York, S. S.; Boesch, S. E.; Wheeler, R. A.; Frech, R., Vibrational Assignments for High Molecular Weight Linear Polyethylenimine (LPEI) Based on Monomeric and Tetrameric Model Compounds. *Macromolecules* **2003**, *36*, 7348-7351.
35. Lakard, S.; Herlem, G.; Lakard, B.; Fahys, B., Theoretical Study of the Vibrational Spectra of Polyethylenimine and Polypropylenimine. *J. Mol. Struc-THEOCHEM.* **2004**, *685*, 83-87.
36. Socrates, G., *Infrared and Raman Characteristic Group Frequencies: Tables and Charts*; Wiley, 2004.
37. Lappi, S. E.; Smith, B.; Franzen, S., Infrared Spectra of $H_2{}^{16}O$, $H_2{}^{18}O$ and D_2O in the Liquid Phase by Single-Pass Attenuated Total Internal Reflection Spectroscopy. *Spectrochim. Acta Mol. Biomol. Spectrosc.* **2004**, *60*, 2611-2619.
38. Yu, J.; Chuang, S. S. C., The Role of Water in CO_2 Capture by Amine. *Ind. Eng. Chem. Res.* **2017**.
39. Khanna, R. K.; Moore, M. H., Carbamic Acid: Molecular Structure and Ir Spectra. *Spectrochim. Acta Mol. Biomol. Spectrosc.* **1999**, *55*, 961-967.
40. Mallapragada, S. K.; Narasimhan, B., Infrared Spectroscopy in Analysis of Polymer Crystallinity. In *Encyclopedia of Analytical Chemistry*, John Wiley & Sons, Ltd: 2006.
41. Kim, H.-J.; Chaikittisilp, W.; Jang, K.-S.; Didas, S. A.; Johnson, J. R.; Koros, W. J.; Nair, S.; Jones, C. W., Aziridine-Functionalized Mesoporous Silica Membranes on Polymeric Hollow Fibers: Synthesis and Single-Component CO_2 and N_2 Permeation Properties. *Ind. Eng. Chem. Res.* **2015**, *54*, 4407-4413.
42. Williams, L., Determination of Hansen Solubility Parameter Values for Carbon Dioxide. In *Hansen Solubility Parameters*, CRC Press: 2007; pp 177-201.

TOC Graphic

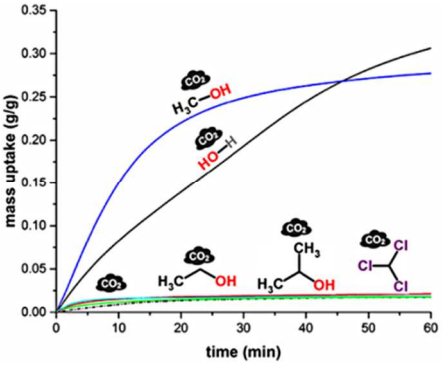
mass uptake (g/g)
time (min)
0.00
0.05
0.10
0.15
0.20
0.25
0.30
0.35
0
10
20
30
40
50
60
CO2
H3C—OH
HO—H
H3C
OH
CH3
Cl
Cl
Cl